24th COBEM - 2017

24th ABCM International Congress of Mechanical Engineering
December 3-8, 2017, Curitiba, PR, Brazil

COBEM-2017-1535
IDENTIFICATION OF THREE-DIMENSIONAL EQUIVALENT MATERIAL PROPERTIES FOR LAMINATED DISKS PACK OF ELECTRIC MACHINE STATORS WITH STRESS-STIFFENING EFFECT

Jean Carlos Marcon
Arcanjo Lenzi
Olavo M. Silva
Federal University of Santa Catarina, Department of Mechanical Engineering, Florianópolis, Brazil
jean.marcon@lva.ufsc.br, arcanjo@lva.ufsc.br, olavo@lva.ufsc.br

Abstract. *Laminated structures can be represented computationally by the finite element method using the homogenization procedure, which consists of the adjustment of equivalent orthotropic properties to a homogeneous structure. The application occurs in stators of electric machines composed of stacked laminated disks connected to each other through windings and other fastening components. This paper describes the characterization of a typical laminated stator through the application of the homogenization method to the magnetic core and consideration of the effect of winding contour conditions and screw joints. Two simplified three-dimensional models for the stator were compared. The first considers the application of a typical tightening of the fastening screws and the presence of a homogeneous isotropic volume representing the winding. The second considers the effect of the boundary condition of the winding on the region of the teeth of the nucleus in order to reduce the degrees of freedom of the complete model. The coupling between the components is accomplished through the application of modal synthesis methods, which require the definition of the surfaces and the type of connection between the components. The obtainment of the set of equivalent orthotropic properties is based on the minimization of residues related to the difference between the natural and experimental frequencies in the range of 0 to 10 kHz. This was carried out using the multi-objective genetic algorithm (MOGA) method was used in conjunction with commercial Ansys® software. Both models presented satisfactory experimental correlation. The simplified model demonstrated limitations of representativeness emphasized in specific frequency bands.*

Keywords: *Finite element method, model updating, electric machines.*

1. INTRODUCTION

Laminated structures such as the stator of an electric motor (Fig. 1) need to be analyzed dynamically in the design phase, preceding industrial application. Modeling complex structures like this can be difficult in the case of unfamiliarity of the mounting properties. For this reason, homogenization methods have been used to recreate the behavior of a heterogeneous structure, reducing the multiplicity of the properties of its components and the number of degrees of freedom of the numerical model (Kalamkarov; Andrianov; Danishev'kyy, 2009; Millithaler, *et al.*, 2015). Their application has proved to be satisfactory in the modeling of composite materials (Kalamkarov; Andrianov; Danishevs'kyy, 2009) and laminated stators (Gomes, 2014; Millithaler, et al., 2015 and Vargas, 2017).

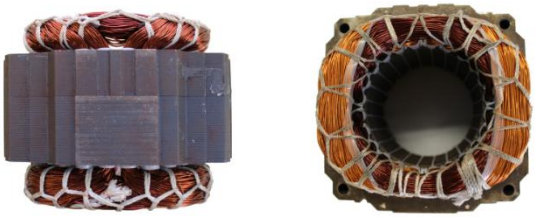

Figure 1. Stator and winding.

This paper describes a methodology for the characterization of electric machine stators composed of connections in conjunction with the homogenization method. The stator of an electric motor, shown in Fig. 1, was used in the development of this methodology. The correlation methods adopted in the model adjustment process and the linear stress-strain law taken into account in the process of determining the equivalent orthotropic properties of the laminated disks pack are presented.

1.1 Correlation methods

Correlation methods applied to the model fitting take into account a comparison between the natural frequencies and numerical and experimental frequency response functions (FRFs) (Mothershead and Friswell, 1993). For a comparison of the p pairs of numerical natural frequencies ω_p^N and experimental frequencies ω_p^E a relative difference can be quantitatively adopted, as given by Eq. (1).

$$\Delta\omega_n\left(\omega_p^N, \omega_p^E\right) = \frac{\omega_p^N - \omega_p^E}{\omega_p^E} . \tag{1}$$

Another common way to correlate natural frequencies is to calculate the average deviation $\overline{\Delta\omega_n}$, given by the simple average of the module of the individual deviations of the natural frequency pairs p, as shown in Eq. (2):

$$\overline{\Delta\omega_n} = \frac{1}{N_p}\sum_{p=1}^{N_p}\left|\Delta\omega_n\left(\omega_p^N, \omega_p^E\right)\right| . \tag{2}$$

Allemang and Brown (1982) recommended calculating an overall divergence between the pairs of natural frequencies, as indicated in Eq. (3):

$$\ell_\omega = \sqrt{\sum_{p=1}^{N}\frac{(\omega_p^N - \omega_p^E)^2}{(\omega_p^E)^2}} . \tag{3}$$

In addition, it is possible to correlate the numerical and experimental modal forms corresponding to the natural frequencies selected for the adjustment through the modal assurance criterion (MAC), defined by Eq. (4). For a pair p of eigenvectors (numerical ψ_p^N and experimental ψ_p^E), the closer this parameter is to unity the stronger the correlation between the modal forms will be. In contrast, a value close to zero indicates a weak correlation. In general, a MAC value above 0.7 is satisfactory and, in the case of complex models, values over 0.6 are acceptable (Allemang and Brown, 1982; Millithaler, 2015).

$$MAC\left(\psi_p^N, \psi_p^E\right) = \frac{|\{\psi^N\}_p^T\{\psi^E\}_p|^2}{\{\psi^N\}_p^T\{\psi^N\}_p\{\psi^E\}_p^T\{\psi^E\}_p} . \tag{4}$$

It is also possible to calculate a mean modal assurance correlation ($\overline{MAC}$), for a number of eigenvector pairs N_p, applying Eq. (5):

$$\overline{MAC} = \frac{1}{N_p}\sum_{p=1}^{N_p} MAC\left(\psi_p^N, \psi_p^E\right) . \tag{5}$$

In addition to comparing natural frequencies and modes of vibration, a comparison between numerical and experimental FRFs provides information on the representativeness of the fitted models and this will also be adopted as an evaluation criterion.

Iterative methods of updating models have been widely studied and applied to vibroacoustic systems. They are based on minimizing a norm calculated from a ℓ residual. This residual is usually dependent on the difference between pairs p of numerical quantities N and experimental quantities E which, in general, is associated with the total mass (Eq. (6)) and the natural frequency (Eq. (7)).

$$\ell_m = m^N - m^E , \tag{6}$$

$$\{\ell_{\omega_p}\} = \frac{\omega_p^N - \omega_p^E}{\omega_p^E} . \tag{7}$$

In the model fitting process, the residuals of the natural frequencies are minimized using a multi-objective genetic algorithm (MOGA), the input parameters being related to the physical properties of the component material, for instance, the modulus of elasticity and the Poisson coefficient.

The first step is to perform a sensitivity analysis, in which appropriate maximum and minimum values are defined for the properties to be adjusted. Subsequently, the total number of individuals of the initial population (set of properties) is defined, which will be randomly generated for the beginning of the analysis. The initial population of the input parameter is tested and based on the results the iterative process begins. In this step, there are combinations and mutations between the selected candidates and results closer to the goal are reached at each iteration. The minimization of the residuals between the numerical results and the reference experimental parameters (natural frequencies) occurs at each iteration until reaching convergence.

In this way, the numerical model was calibrated to represent the dynamic behavior of the stator. After adjusting the natural frequencies, the correlation of the modal shapes and the numerical and experimental FRFs was performed. The Ansys® commercial software is used for the numerical solution of the dynamic problems presented.

1.2 Stress-strain law

In general, a solid body can have six possible stress σ and strain ε components. The simplest linear relationship between these components is of the form $\{\sigma\} = [C]\{\varepsilon\}$, where $[C]$ is an elastic matrix, $\{\sigma\}$ is the stress tensor and $\{\varepsilon\}$ is the strain tensor. Thus, Hooke's law for anisotropic materials can be represented by Eq. (8), which presents 21 independent elastic constants C_{ij} (Tadmor, Miller and Elliott, 2012).

$$\begin{Bmatrix} \sigma_{11} \\ \sigma_{22} \\ \sigma_{33} \\ \sigma_{23} \\ \sigma_{31} \\ \sigma_{12} \end{Bmatrix} = \begin{bmatrix} C_{11} & \cdots & C_{16} \\ \vdots & \ddots & \vdots \\ C_{61} & \cdots & C_{66} \end{bmatrix} \begin{Bmatrix} \varepsilon_{11} \\ \varepsilon_{22} \\ \varepsilon_{33} \\ \varepsilon_{23} \\ \varepsilon_{31} \\ \varepsilon_{12} \end{Bmatrix}. \tag{8}$$

In many practical problems, the materials have planes of symmetry along three orthogonal directions, which give them orthotropic properties. Thus, Eq. (8) can be simplified and the inverse of the elasticity matrix $[C]$ is given by the conformity matrix $[D]$, represented by Eq. (9):

$$[D] = \begin{bmatrix} \frac{1}{E_{11}} & \frac{-\nu_{12}}{E_{11}} & \frac{-\nu_{31}}{E_{33}} & 0 & 0 & 0 \\ \frac{-\nu_{12}}{E_{11}} & \frac{1}{E_{22}} & \frac{-\nu_{23}}{E_{22}} & 0 & 0 & 0 \\ \frac{-\nu_{31}}{E_{33}} & \frac{-\nu_{23}}{E_{22}} & \frac{1}{E_{33}} & 0 & 0 & 0 \\ 0 & 0 & 0 & \frac{1}{2G_{23}} & 0 & 0 \\ 0 & 0 & 0 & 0 & \frac{1}{2G_{31}} & 0 \\ 0 & 0 & 0 & 0 & 0 & \frac{1}{2G_{12}} \end{bmatrix}, \tag{9}$$

in which E_{ii} is the Young's modulus in the main directions of the material; G_{ij} is the shear modulus; and ν_{ij} is the Poisson ratio, which obeys the relations of Eq. (10):

$$\nu_{ij} = \nu_{ji} \frac{E_{ii}}{E_{jj}}. \tag{10}$$

For isotropic materials the properties do not vary with the orthogonal direction and are simply represented by E, ν and G and the matrix $[D]$ can be simplified.

In addition to the field of isotropic properties, Ansys® commercial software has an input interface for orthotropic material parameters, making its application quite extensive. For each orthotropic elastic linear material, nine properties can be adjusted, notably the elastic moduli E_x, E_y and E_z, the Poisson ratios ν_{xy}, ν_{yz} and ν_{zx} and shear moduli G_{xy}, G_{yz} and G_{zx}. The x, y and z axes of the Cartesian coordinate system (or r, θ and z of the cylindrical coordinate system) correspond to indices 1, 2 and 3 of Eqs. (8) and (9), respectively. In the case of isotropic materials, the set of properties is restricted to E, G and ν.

At each iteration of the model adjustment process, some restrictions are imposed on the elastic constants of the orthotropic material. The first condition states that the elastic constants are positive, as indicated by Eq. (11). The second considers that the determinant of the matrix $[D]$ must also be positive, according to Eq. (12). Finally, the previous requirements lead to the relations of Eq. (13).

$$E_{11}, E_{22}, E_{33}, G_{12}, G_{23}, G_{31} > 0, \tag{11}$$

$$1-\nu_{12}\nu_{21}-\nu_{31}\nu_{13}-\nu_{23}\nu_{32}-2\nu_{21}\nu_{32}\nu_{13}>0\,, \tag{12}$$

$$\nu_{21}<\sqrt{\frac{E_{22}}{E_{11}}}\,;\ \nu_{32}<\sqrt{\frac{E_{33}}{E_{22}}}\,;\ \nu_{13}<\sqrt{\frac{E_{11}}{E_{33}}}\,. \tag{13}$$

The next section describes the experimental procedure used for the determination of the modal parameters of the electric motor stator and the characterization of the laminated disks of which it is comprised.

2. EXPERIMENTAL PROCEDURE

In order to reduce the number of variables in the stator model adjustment process, seven laminated disks were characterized to evaluate the feasibility of fixing the modulus of elasticity in the two directions of the radial plane and the respective Poisson coefficient. In this procedure, the laminated disks were hung in the support represented in Fig. 2 and impacted by a hammer at the response measurement point. Through the FRFs obtained by the fixation of a uniaxial accelerometer, one can analyze the manufacturing variability between the laminated disks and adjust the numerical model to estimate their equivalent properties.

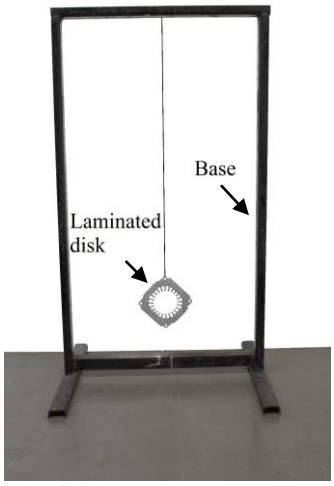

Figure 2. Experimental setup used for laminated disk analysis.

The configuration used in the experimental modal analysis is shown in Figs. 3a and 3b. Figure 3a shows the shaker connection with the stator for the application of excitement using white noise in the radial direction of the component. The connection is made through the stinger, the force signals are measured by the load cell and the acceleration signals are measured with triaxial accelerometers at 50 points, as indicated in Fig. 3c. A second transverse excitation was adopted as a reference, as shown in Fig. 3b. The stator is suspended by a support.

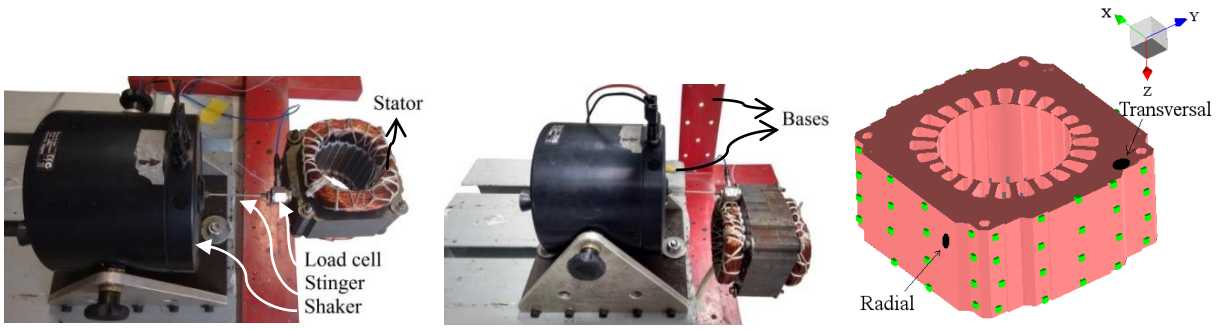

(a) (b) (c)

Figure 3. Experimental setup for modal analysis of the stator: (a) excitation in the radial direction; (b) excitation in the transversal direction; and (c) experimental mesh with 50 points.

The numerical models presented in the next section were fitted using the modal parameters obtained experimentally. In this procedure, the concepts presented in sections 1.1 and 1.2 were applied.

3. COMPUTATIONAL PROCEDURE

In order to estimate the physical properties of the laminated disk and to associate them with the radial behavior of the stator, a model was proposed through the application of the finite element method, represented in Fig. 4, for the direct correlation between the numerical and experimental FRFs (verify reference point). In the numerical model, the laminated disk was considered as a homogeneous isotropic material. The properties were fitted to the same element (quadratic hexahedral) used in the laminated disks pack of the stator model. Only a small variation in the modulus of elasticity of the isotropic laminated disk was verified when a triangular linear element was adopted.

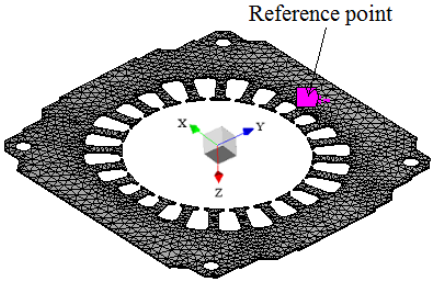

Figure 4. Numerical model of the laminated disk and reference point specification.

With the application of the homogenization method, two stator models were based on a simplified geometry (solid body representing the set of overlapping laminated disks), which considers the contour condition of the screws and the winding. The two models can be seen in Figs. 5 and 6b. The first considers the set of laminated disks as a continuous structure and the winding is represented by an equivalent volume, fixed between the teeth of the stator, approaching the practical condition. The second presents a simplification, considering the effect of the winding on the teeth of the magnetic core. In this case, distinct orthotropic properties are determined for the two parts of the magnetic core. The inertial effect of the winding was approximated by an increase in the density in the region of the stator teeth, and in the radial plane (x-y) of the teeth the stiffness effect was introduced through an increase in the stiffness. Consequently, the shear modulus also changed in the region of the teeth, in relation to the external region (Fig. 6b).

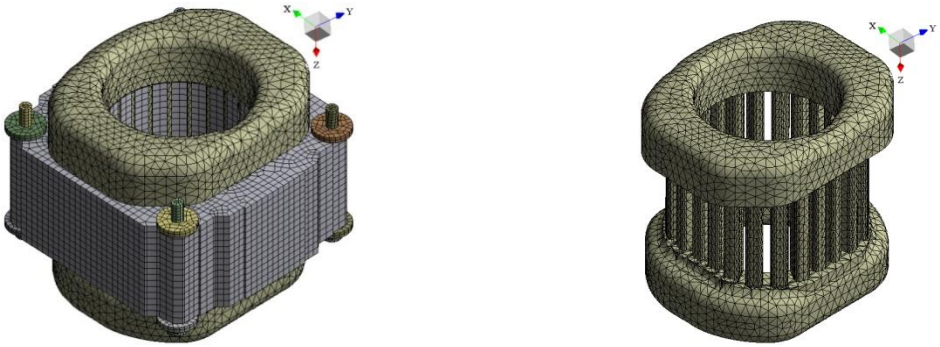

(a) (b)

Figure 5. (a) Full numerical model of the stator, with the physical presence of the winding and (b) isotropic volume of the winding.

The densities used in the model are calibrated from experimental data and the use of Eq. 14, which gives ρ as a function of the total mass m_{tot} and the total volume V_{tot} of the components.

$$\rho = \frac{m_{tot}}{V_{tot}}. \tag{14}$$

In both numerical models, a quadratic hexahedral element was used to represent the equivalent volume of the laminated disks. In the complete model, the winding was represented with a quadratic tetrahedral element. The connections of the components of both models (washers and screws) were considered to have typical isotropic properties, with quadratic hexahedral elements.

The contact interfaces between the components of both models are shown in Fig. 6a. The lower degree of contact between the washer and the screw was defined as Bonded, with an Augmented Lagrange formulation. To simplify the connection between the nut, the washer and the bolt, the nut was omitted. The screw was connected directly to the

washer by a Bonded connection, defined as a multi-point constraint (MPC). The contact between the surfaces of the washer and the laminated disks pack was defined as Frictional, that is, it is considered that there is a friction effect at this interface (as in practice). The coefficient of friction is defined according to empirical data and it is dependent on the physical conditions of the surfaces in contact.

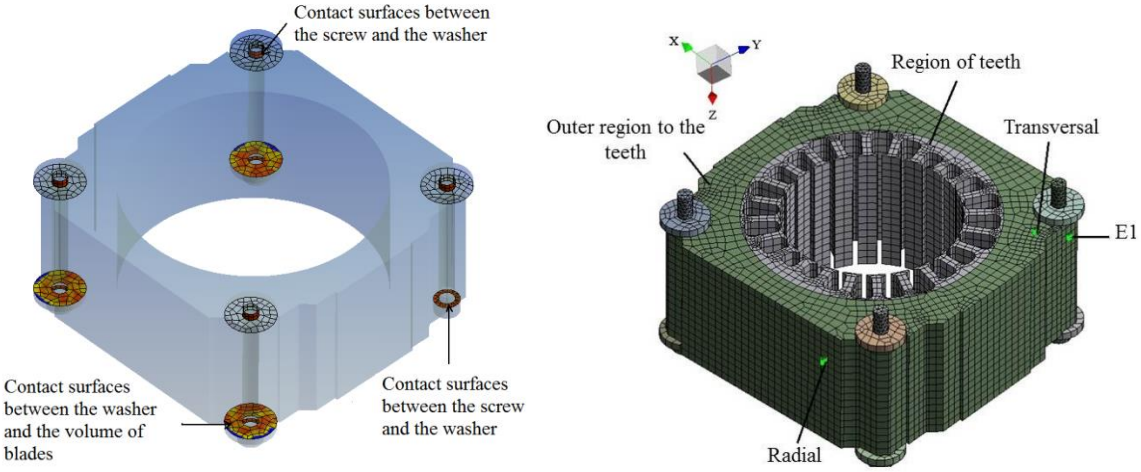

(a) (b)

Figure 6. (a) Specification of contact regions between stator components for both models and (b) simplified numerical stator model.

Although not indicated in Fig. 6a, the Augmented Lagrange formulation was used for the connection between the winding and the stator teeth, in the case of the complete model. These formulations provide greater sensitivity in adjusting the stiffness of the connection.

Since the modal and harmonic analyses are linear, the nonlinear connections used in the models (Augmented Lagrange and Frictional) underwent a linear adaptation. The reference and response points can be seen in Fig. 6b, resembling the experimental set-up shown in Fig. 3c.

The stress-stiffening effect is included in a static analysis that precedes the modal analysis, making an initial estimation of the properties and applying a nominal pre-stress on the screws. The basic relation for the calculation of the normal force of the fastening elements is given in Eq. 15 (Norton, 2004), where F_n is the tensile force, M_a is the tightening moment, d is the diameter of the fastening element and k_a is the torque coefficient, which is dependent on the physical connection conditions.

$$F_n \cong \frac{M_a}{d\,k_a}. \tag{15}$$

The modal analysis of the set is carried out with the pre-stress history and the application of modal synthesis methods (Craig and Bampton, 1968; Craig, 1987; Herting, 1985; Martinez, *et al.*, 1984). These methods provide good modal analysis estimates of several interconnected components, including their connection properties.

4. RESULTS AND DISCUSSION

The first model adjusted was that of the laminated disks. With the aid of the Genetic Algorithm, the first eight peaks of the numerical FRF were approximated to the equivalents of the average experimental FRF, using as the convergence criterion a limit value for the sum of the relative difference. A comparison between the FRFs can be observed in Fig. 7. It is evident that the adjustment loses precision in terms of amplitude from 6 kHz (influence of the experimental contour condition) and that the variation of the vibrational behavior due to the manufacturing is small. The mass of the laminated disks was calibrated experimentally.

To obtain the optimal physical properties of the laminated disk (modulus of elasticity and Poisson coefficient), an initial population of 130 candidates, with 50 samples per iteration, was adopted in order to obtain satisfactory solutions for a total of 20 iterations. The final solutions were obtained after 516 evaluations and 10 iterations.

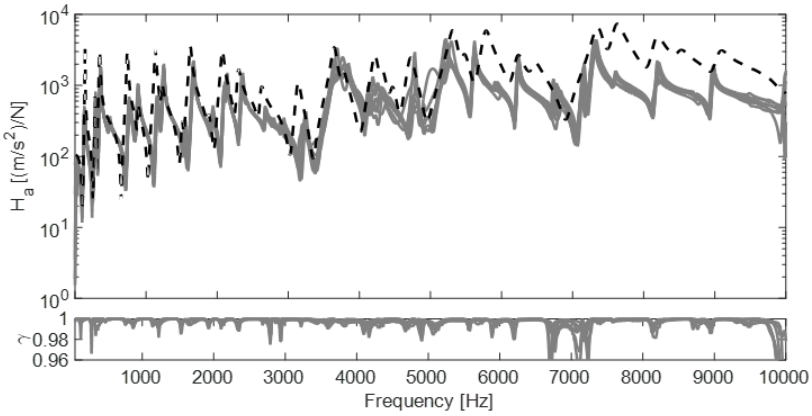

Figure 7. Numerical model of the laminated disk set in black (dashed line) and the experimental FRFs in gray (continuous line) as a reference.

Table 1 shows the natural frequency values for the experimental and numerical reference FRFs, with the respective minimized relative errors. Both the average deviation of 2.8% and the overall divergence of 11.7% are satisfactory.

Table 1. Comparison between the numerical and experimental natural frequencies of the first eight peaks of the reference point FRF after the adjustment of the laminated disk model.

Order	ω^E **(Hz)**	ω^N **(Hz)**	$\Delta\omega_n$ **(%)**
1	129.9	116.8	-10.2
2	290.2	280.3	-3.4
3	360.3	345.3	-4.1
4	490.0	487.4	-0.5
5	769.6	773.6	0.5
6	890.3	882.8	-0.8
7	1160.5	1172.1	1.0
8	1240.0	1218.0	-1.8
Average (%):			2.8
ℓ_ω **(%):**			11.7

Wang (2002) conducted an experimental study on the effects of the vibration between connected annular laminated disks for comparison with the results of the equivalent finite element model. He made vacuum coupling comparisons to investigate the effect of the thickness and the number of connected laminated disks, eliminating the effect of the physical presence of the screws. It was found that the effects of the tightening and the number of laminated disks provide the transverse vibration modes more effectively when compared to the radial modal shapes, which is consistent with the results obtained herein. These effects are directly related to the damping and shearing of the laminated structure. The same author also identified the projection of the individual modes of a laminated disk on the overall modes of the set. Therefore, the first step in the verification of the dynamic behavior and adjustment of a numerical model of a stator should be the investigation of the laminated disk itself.

As Wang (2002) observed, some modal shapes of a laminated disk may have characteristics very close to those identified in the case of multiple laminated disk coupling. Figure 8 shows some transversal and radial modal shapes of the laminated disk, numerically found, which are similar to those obtained experimentally with the stator. Although the transverse vibration modes (Figures 8a, 8b and 8c) occur at very different frequencies, it can be noted that the radial vibration modes (Figures 8d and 8e) appear at frequencies very close to those corresponding to the set of stator laminated disks. These modal shapes should be observed on the stator after the model adjustment.

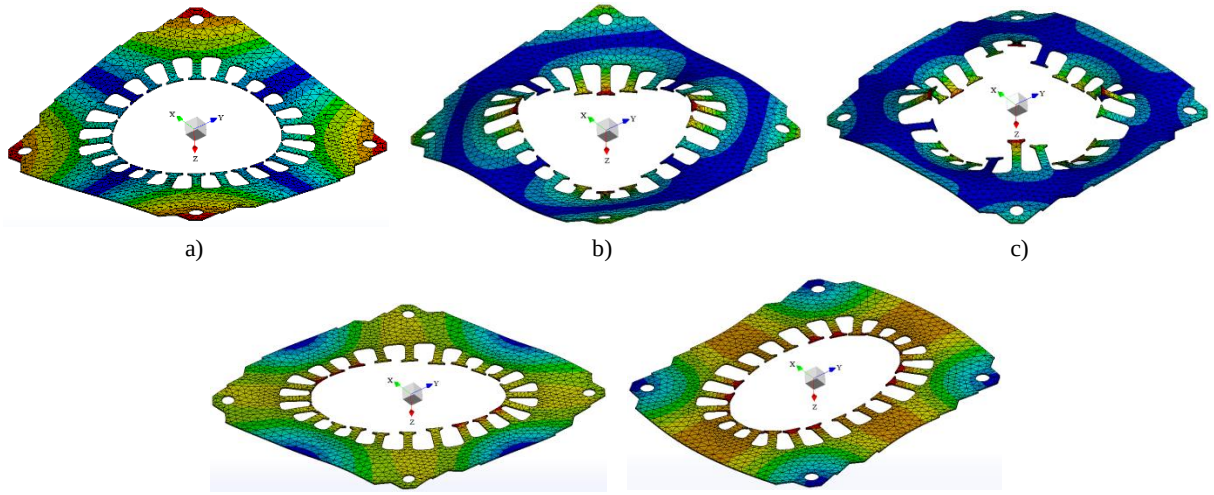

a) b) c)

d) e)

Figure 8. Modal shapes of the laminated disk, whose characteristics are repeated on the stator laminated disks pack, according to experimental modal analysis.

Due to the proximity of the modal characteristics, the isotropic properties adjusted for the laminated disk were used in the radial plane (x-y) of the laminated disks pack of the complete stator model (E_x, E_y, ν_{xy} and ρ), and in the region external to the teeth of the simplified model. Thus, in addition to the density, which can be calibrated directly with the weight, the fixed adjustment parameters include the Poisson coefficient and the modulus of elasticity in the radial plane. This simplification eliminates the need to represent the contact between the laminated disks and allows the use of larger finite elements, enabling the modeling. Another benefit is a reduction of the number of variables to be estimated in the adjustment and optimization of the numerical model.

In order to be as faithful as possible to the physical constitution, each component of the stator was characterized separately. The washers, screws and laminated disks were characterized and then added to the volume representing the set of laminated disks. The homogenization method was also used to represent the copper coil through a homogeneous volume with equivalent isotropic properties.

After an initial sensitivity analysis and the restriction of the lateral limits of the properties (minimum and maximum) to within a range of suitable values, the complete stator model (Fig. 5a) was adjusted based on five experimentally identified modal shapes. According to Table 2, the relative maximum and minimum differences between the numerical and experimental natural frequencies were -5.5% and 0.9%, respectively. The overall divergence is 7.8% and the average is 2.9%.

Table 2. Correlation between the numerical and experimental natural frequencies, for the stator model with the equivalent volume of the winding.

Order	ω^E **(Hz)**	ω^N **(Hz)**	$\Delta\omega_n$ **(%)**
1	1084.0	1024.1	-5.5
2	1477.3	1543.7	4.5
3	3621.4	3582.8	-1.1
4	3848.4	3884.4	0.9
5	5129.3	4990.1	-2.7
Average (%)			2.9
ℓ_ω **(%):**			7.8

The damping factor was calibrated after matching with the numerical and experimental FRFs, and its value is consistent with the results obtained experimentally. It should be noted that there may be other sets of parameters that represent the stator satisfactorily.

The natural frequencies that are most sensitive to the transversal shear moduli are related to the transverse modal shapes and shear modal shapes in the radial plane. The natural frequencies corresponding to the radial modal shapes are more sensitive to the shear modulus in the same plane. The Poisson coefficient did not show a significant influence on the reference frequencies.

In order to reduce the number of degrees of freedom of the complete model, the simplified model that considers only the effect of the winding contour condition on the stator teeth was adjusted (Fig. 6b). The correlation between the natural frequencies and the numerical and experimental modal shapes of the simplified model is shown in Table 3. The overall divergence between the natural frequencies is 8.6% and the mean deviation is 3.0%, with a maximum deviation of -6.8% and a minimum of 0.8%. The corresponding MAC values are also shown in Table 3, with an average magnitude of 66.0% (maximum of 83.5% and minimum of 59.1%). Despite the experimental limitations that can interfere in the quality of the modal reference parameters obtained, the adjustment is considered satisfactory.

Table 3. Correlation between the natural frequencies and modal numerical and experimental shapes for the stator model without the physical presence of the winding.

Order	ω^E **(Hz)**	ω^N **(Hz)**	$\Delta\omega_n$ **(%)**	**MAC (%)**
1	1084.0	1136.9	4.9	83.5
2	1477.3	1489.8	0.8	62.4
3	3621.4	3656.5	1.0	63.8
4	3848.4	3796.2	-1.4	61.3
5	5129.3	4780.0	-6.8	59.1
Average (%)			3.0	66.0
ℓ_ω **(%):**			8.6	

Following the same procedure described for the complete model, the same properties of the laminated disk were maintained in the x-y plane (radial). The remainder of the properties were adjusted, maintaining the division of the outer part of the laminated disk volume and the inner part, which corresponds to the region of the teeth of the magnetic core (Fig. 6b).

The set of properties determined is consistent with several previous studies in which the laminated stators were investigated. Although the models studied by Wang and Lai (1999), Millithaler *et al.* (2015) and Millithaler (2015) are geometrically different, it was found that the modulus of elasticity in the radial direction is usually greater than the same parameter in the axial direction. Similarly, in general, the shear modulus and Poisson coefficient in the radial plane are larger compared to the same parameters in the two orthogonal directions.

The main difference between the two calibrated models is the presence of the main modal forms of the winding in the 300 to 900 Hz band. The computational solution is faster for the simplified model, which does not consider the coupling and winding vibration modes.

For frequencies higher than 900 Hz, the physical presence of the winding can be neglected, since the dynamic behavior is very close to that of the simplified model. The absence of the winding significantly reduces the modal density of the part, due to the exclusion of modes located at frequencies above 900 Hz. Due to the difficulty associated with modeling a set of copper wires, this approximation by a homogeneous isotropic material proved to be representative.

Point E1 in Fig. 6b was used to obtain a response and two reference points (transversal and radial) for matching between numerical and experimental FRFs. These comparisons can be seen in Figs. 9 and 10, in which the FRFs in black are the numerical values, where the continuous line represents the complete model and the dashed line corresponds to the simplified model of the stator. The experimental FRFs in gray relate to the samples of seven stators. The FRFs present good correlations, and the numerical results are within the range of experimental variability obtained. In this case, a constant damping factor was used. However, modal damping factors or optimized Rayleigh damping factors can be specified for the calibration of response levels, in concordance with the experimental results.

As mentioned above, due to the absence of the physical volume of the winding, the simplified numerical model loses accuracy in the frequency range between 300 and 900 Hz. Both numerical models show low sensitivity in representing the physical process of detachment of the laminated disks, particularly above 7 kHz.

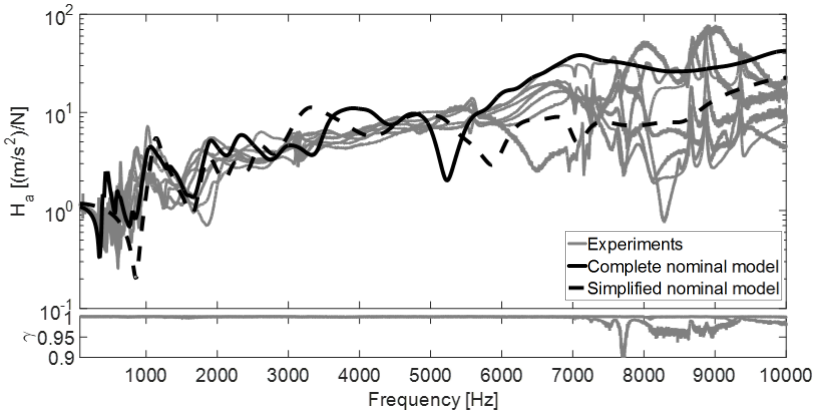

Figure 8. Comparison between the numerical and experimental FRF values for transversal excitation (z direction) and response measurement at point E1 (z direction).

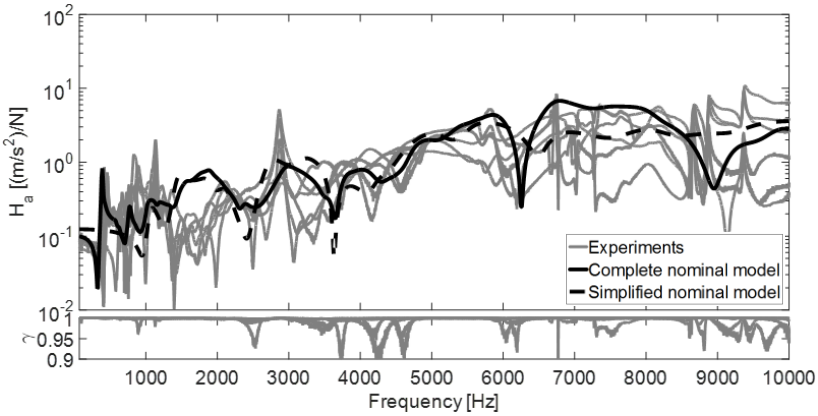

Figure 9. Comparison between the numerical and experimental FRF values for radial excitation (y direction) and response measurement at point E1 (z direction).

On comparing the FRFs shown in gray in the graphs, it can be noted that the experimental variability is accentuated. Considering that the properties of the laminated disks vary little from one stator to the other, the observed variability between the stators is mainly associated with the uncertainties of the tightening torque of the screws and the winding, that is, the stiffness oscillations of fixation, of mass and, therefore, of damping. For the set of eight stators evaluated, the largest mass variation was 27.0 g (in relation to the average) associated with the winding. This shows that the effect of mass fluctuations is reduced compared to variations in the stiffness and damping.

5. CONCLUSIONS

Satisfactory numerical representations were obtained through the application of the homogenization method for the two proposed numerical models, with addition of the pre-stress effect of the screws and the connection between the components. For all property settings, the average deviation between the numerical and experimental natural frequencies was equal to or less than 3.0%. These numerical models can be used in many practical applications with relatively low computational cost. However, depending on the purpose of the study, a more detailed representation of the connection properties and the physical phenomenon involved may be required, resulting in a considerable increase in the number of degrees of freedom of the models.

The simplified numerical model of the laminated stator presented limitations of representativeness in the frequency range between 300 and 900 Hz due to the absence of the modal shapes of the winding. Although diverging from the physical reality, properties such as the modulus of elasticity and density, measured for the region of the teeth in the simplified model, impart a dynamic behavior close to those of the complete model and the real component.

The two numerical models do not accurately describe the discontinuities of the laminated disks, particularly at frequencies above 7 kHz. It should be noted that contour condition effects interfered in the experimental process of obtaining the modal parameters, mainly due to the complexity of the component tested. The damping can also be optimized, as a function of the frequency, to obtain a better correlation between the numerical and experimental FRFs.

The pre-stress effect applied to the stator screws proved to be important to better characterize the modal forms of numerical models and to change the local stiffness around the connections due to the stress-stiffening effect. Modal synthesis performed with the commercial Ansys® software was found to be adequate, enabling computational vibroacoustic analysis.

6. ACKNOWLEDGEMENTS

The first author received financial support from the Brazilian governmental agency CNPq, which is gratefully acknowledged.

7. REFERENCES

Allemang, R. J.; Brown, D. L., 1982, Correlation coefficient for modal vector analysis, Proceedings of the 1st International Modal Analysis Conference, Orlando: [s.n.], p. 110-116.

Craig, R. R., 1987, A review of time domain and frequency domain component modal synthesis methods, International journal of analytical and experimental modal analysis, p. 59-72.

Gomes, L. K. C. R. Análise dinâmica do estator de um motor elétrico. Thesis (Master's) - Universidade Federal de Santa Catarina. ed. Florianópolis: [s.n.], 2014.

Craig, R. R.; Bampton, M. D. D., 1968, Coupling of substructures for dynamic analysis, AIAA Journal, p. 1313-1319.

Herting, D. N., 1985, A general purpose, multi-stage, component modal synthesis method, Finite elements in analysis and design, p. 153-164.

Kalamkarov, A. L.; Andrianov, I. V.; Danishev'kyy, V. V., 2009, Asymptotic homogenization of composite materials and structures, American Society of Mechanical Engineers, n. 3, p. 20.

Martinez, D. R. et al., 1984, Combined experimental/analytical modeling using component mode synthesis, AIAA, p. 140-152.

Millithaler, P., 2015, Dynamic behaviour of electric machine stators: modelling guidelines for efficient finite-element simulations and design specifications for noise reduction, Thesis (PhD) - l'Université de Franche-Comté, ed. Besançon: [s.n.].

Millithaler, P. et al., 2015, Structural dynamics of electric machine stators: Modelling guidelines and identification of three-dimensional equivalent material properties for multi-layered orthotropic laminates, Journal of Sound and Vibration, p. 185-205.

Mothershead, J. E.; Friswell, M. I., 1993, Model updating in structural dynamics: a survey, Journal of Sound and Vibration, p. 347-375.

Norton, R. L. Projeto de máquinas: uma abordagem integrada. 2. ed. Porto Alegre: Bookman, 2004. ISBN 978-85-363-0273-7.

Tadmor, E. B.; Miller, R. E.; Elliott, R. S. Continuum Mechanics and Thermodynamics. New York: Cambridge University Press, 2012. ISBN 978-1-107-00826-7.

Vargas, J. G. Análise das fontes de ruído de uma lavadoura de roupa. Thesis (Master's) - Universidade Federal de Santa Catarina. ed. Florianópolis: [s.n.], 2017

Wang, C.; Lai, J. C. S. Vibration analysis of an induction motor. Journal of sound and vibration, Canberra, 28 January 1999. 733-756.

Wang, H. Experimental study of vibration behavior of laminated annular disks. Acoustical Society of America, 4 April 2002.

8. RESPONSIBILITY NOTICE

The authors are solely responsible for the printed material included in this paper.